IOP Conf. Series: Journal of Physics: Conf. Series **796** (2017) 012013 doi:10.1088/1742-6596/796/1/012013

Numerical investigation on forced convection in rectangular cross section micro-channels with nanofluids

B Buonomo*, L Cirillo, O Manca, S Nardini, S Tamburrino

Dipartimento di Ingegneria Industriale e dell'Informazione, Seconda Università degli Studi di Napoli (SUN), Via Roma 29, Aversa (CE), 81031, Italia

*Corresponding author: buonomo.bernardo@unina2.it

Abstract. In this paper a numerical investigation on laminar forced convection flow of a water–Al_2O_3 nanofluid in a rectangular microchannel is accomplished. A constant and uniform heat flux on the external surfaces has been applied and a single-phase model approach has been employed. The analysis has been performed in steady state regime for particle size in nanofluids equal to 38 nm. The CFD commercial code Fluent has been employed in order to solve the 3-D numerical model. The geometrical configuration under consideration consists in a duct with a rectangular shaped crossing area. A steady laminar flow and different nanoparticle volume fractions have been considered. The base fluid is water and nanoparticles are made up of alumina (Al_2O_3). The length the edge and height of the duct are 0.030 m, 1.7 $x10^{-7}$ and 1.1 $x10^{-7}$ m, respectively. Results are presented in terms of temperature and velocity distributions, surface shear stress and heat transfer convective coefficient, Nusselt number and required pumping power profiles. Comparison with results related to the fluid dynamic and thermal behaviors are carried out in order to evaluate the enhancement due to the presence of nanoparticles in terms of volumetric concentration.

1. Introduction

The heat transfer in fluids is very crucial for industrial applications, especially for heating or cooling operation. Convective heat transfer can be enhanced passively by changing flow geometry, by enhancing the thermal conductivity of the working fluid, or putting another material in the system with high value of the thermal conductivity. An innovative method of enhancement of thermal conductivity of base fluids is to insert nanoparticles. In fact, several investigations have been accomplished on the microchannel heat sink using nanofluids [1]. The nanofluid in a microchannel heat exchanger was studied by Lee and Choi [2] and they confirmed that the nanofluid enhances the cooling rate respect to the pure water and liquid nitrogen.

A numerical study on the laminar forced convection in microchannel with nanofluid is carried out in Koo and Kleinstreuer [3] considering two types of nanofluids, CuO/ethylene glycol and CuO/water. They found that nanoparticles with a high value of thermal conductivity enhance the heat transfer. An experimental investigation with nanofluid in microchannel is realized by Chied and Chuang [4]. The results showed that there is a slight increase of the pressure drop due to the presence of the nanoparticles but the heat transfer is improved. The turbulent forced convection in duct with nanofluid was studied in numerical way in Behzadmehr et al. [5]. The nanofluid is modelled employing the two phase mixture model and a comparison with the experimental values is made. The

results showed that the two phase mixture model is more accurate than the single phase model. Moreover the use of nanofluid improves the Nusselt number and it seems that the friction factor is not affected. A study on the rectangular microchannels is accomplished by Jung et al. [6], where they found an improvement of the convective heat transfer coefficient but a worsening of the friction factor, in fact the convective heat transfer coefficient of nanofluid is increased of 32% respect to the convectional water. A numerical study on Al_2O_3/water nanofluid in microchannel is carried out in Bhattacharya et al. [7]. The study showed that in the laminar flow the heat transfer coefficient for nanofluid increase with the Reynolds number. Chen and Ding [8] studied the thermal performance of a microchannel heat sink using a porous medium model with Forchheimer-Brinkman-Darcy equation for the fluid flow and the Local thermal non-equilibrium model for the heat transfer. The viscous dissipation effect is taken into account and the results showed that the heat transfer decreases as the particle's diameter increases.

A numerical 3D simulation for incompressible, steady fluid flow of a trapezoidal microchannel using CuO/water nanofluid is accomplished in Yang et al. [9]. They found that the thermal resistance of nanofluid is smaller than the water and the pressure drop increase slightly using the nanofluid respect to the pure water.

After this short review, it seems that there is a lack of work on forced convection in rectangular microchannels in nanofluids. In this paper, a numerical investigation on laminar forced convection in rectangular microchannel with nanofluids is accomplished, in order to assess thermo-dynamic behavior of the considered geometry by using Al_2O_3/water based nanofluids. The nanofluid is modelled with the single phase model and the system is heated by a constant and uniform heat flux on of the top walls of the duct. Results are presented for different nanoparticle volume concentrations and Reynolds number values.

2. Geometrical model and data reduction

The 3-D numerical model consists of a duct with a rectangular shaped crossing area, showed in Fig. 1a, with length, edge and height respectively equal to 0.030 m, 1.7×10^{-7} m and 1.1×10^{-7} m. The flow in the duct is three-dimensional, steady-state, laminar and incompressible. Thermo-physical properties of the nanofluid are considered constant with temperature except for the density where is assumed the Boussinesq approximation because of the presence of buoyancy force. A constant and uniform heat flux q on the top wall is applied; the others are adiabatic and for the inlet section is assumed a uniform velocity and temperature profile. The analysis has been performed for particle size in nanofluids equal to 38 nm. The geometrical configuration of the cross section is showed in Fig. 1b and the geometrical quantities are summarized in Table 1.

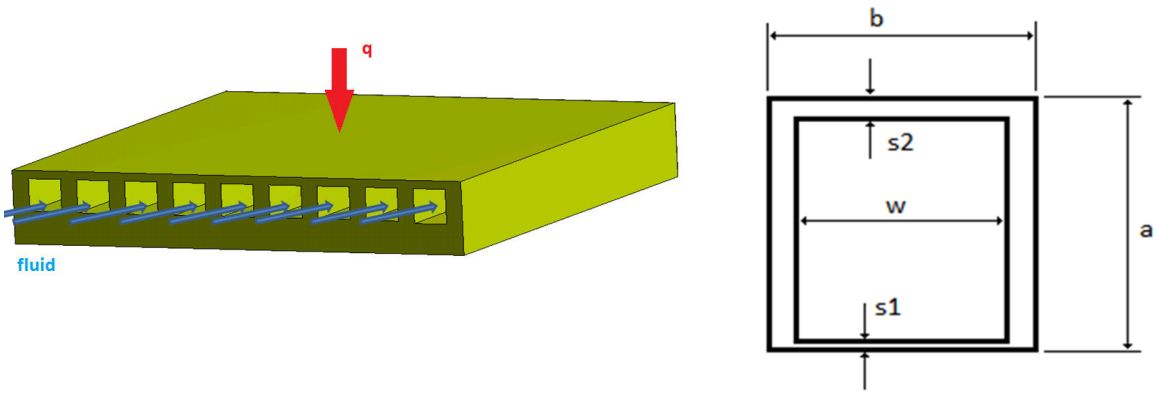

a) b)

Figure 1. a) Schematic presentation of the microchannel heat sink; b) cross-section of microchannel used in the computations.

Table 1. Dimensions of geometrical quantities

a (μm)	*b* (μm)	*w* (μm)	*s1* (μm)	*s2* (μm)
280	447	430	6	10

Continuity:

$$\frac{\partial u}{\partial x}+\frac{\partial v}{\partial y}+\frac{\partial w}{\partial z}=0 \tag{1}$$

Momentum:

$$\left[u\frac{\partial u}{\partial x}+v\frac{\partial u}{\partial y}+w\frac{\partial u}{\partial z}\right]=-\frac{1}{\rho_{nf}}\frac{\partial P}{\partial x}+\nu_{nf}\left[\frac{\partial^2 u}{\partial x^2}+\frac{\partial^2 u}{\partial y^2}+\frac{\partial^2 u}{\partial z^2}\right] \tag{2}$$

$$\left[u\frac{\partial v}{\partial x}+v\frac{\partial v}{\partial y}+w\frac{\partial v}{\partial z}\right]=-\frac{1}{\rho_{nf}}\frac{\partial P}{\partial y}+\nu_{nf}\left[\frac{\partial^2 v}{\partial x^2}+\frac{\partial^2 v}{\partial y^2}+\frac{\partial^2 v}{\partial z^2}\right] \tag{3}$$

$$\left[u\frac{\partial w}{\partial x}+v\frac{\partial w}{\partial y}+w\frac{\partial w}{\partial z}\right]=-\frac{1}{\rho_{nf}}\frac{\partial P}{\partial z}+\nu_{nf}\left[\frac{\partial^2 w}{\partial x^2}+\frac{\partial^2 w}{\partial y^2}+\frac{\partial^2 w}{\partial z^2}\right] \tag{4}$$

Energy for fluid phase:

$$\left(\rho c_p\right)_{nf}\left[u\frac{\partial T_{nf}}{\partial x}+v\frac{\partial T_{nf}}{\partial y}+w\frac{\partial T_{nf}}{\partial z}\right]=\lambda_{nf}\left[\frac{\partial^2 T_{nf}}{\partial x^2}+\frac{\partial^2 T_{nf}}{\partial y^2}+\frac{\partial^2 T_{nf}}{\partial z^2}\right] \tag{5}$$

Energy equation in the solid domain:

$$\frac{\partial^2 T_s}{\partial x^2}+\frac{\partial^2 T_s}{\partial y^2}+\frac{\partial^2 T_s}{\partial z^2}=0 \tag{6}$$

The following boundary conditions are assumed:

- inlet section: uniform velocity and temperature profile;
- outlet section: outflow condition with velocity components and temperature derivatives equal to zero;
- external duct walls: assigned uniform and constant heat flux on the top wall, the others are adiabatic;
- solid-fluid interface: velocity components equal to zero and continuity of the temperature and heat flux.

The dimensionless parameters Reynolds number, Nusselt number and friction factor are considered for the data reduction and they are expressed by the following relations:

$$Re=\frac{Vd_h}{\nu} \tag{7}$$

where V is the average inlet velocity, d_h is the hydraulic diameter.

$$Nu_{av} = \frac{qd_h}{(T_w - T_m)\lambda_{nf}} \tag{8}$$

where q is the heat flux, T_w and T_m represent the average wall and bulk fluid temperatures, respectively.

$$f = 2\Delta P \frac{d_h}{4L} \frac{1}{\rho_{nf} V^2} \tag{9}$$

$$Pr = \frac{\mu c_p}{\lambda} \tag{10}$$

3. Grid independence analysis

The governing equations (1)-(6) with the assumed boundary conditions were solved by means of Fluent 6.3 [10] code. A segregated method was chosen to solve the stationary equations and a second-order upwind scheme was employed for energy and momentum equations. Pressure and velocity were coupled by using SIMPLE coupling scheme. Simulations were considered converged by assuming the convergence criteria of 10^{-4} and 10^{-5} and 10^{-8} for the residuals of continuity, velocity components and energy, respectively. At the inlet section, flow was considered laminar, with a velocity corresponding to the assigned Reynolds number, at a temperature of 293K and ambient pressure conditions. The no-slip condition was applied on the channel walls, which were heated by a uniform and constant heat flux.

A grid dependence test is accomplished to realize the more convenient grid size by monitoring average Nusselt for rectangular microchannel system. Four different unstructured mesh distributions, were tested with water as fluid on the rectangular sectioned duct for *Ti*=293 K, *V*=0.6m/s (*Re*=50) with a uniform heat flux equal to about 75.6 kW/m^2 imposed on the upper surface of the channel in order to perform the grid-independence analysis. They have 70000, 144000, 280000, 480000 and 739000 nodes, respectively. To evaluate the computational grid the Richardson extrapolation was used in terms of Nusselt number. The third grid case (280000 nodes) was adopted because it ensured a good compromise between the computational time and the accuracy requirements. The validation has been then performed by comparing the numerical results, in terms of Nusselt number and friction factor, for *Re*=50 with data from Shah and London [11] for uniform and constant thermal heat flux boundary condition. The reference analytical value is equal to 3.11, while the computation Nusselt number value is 3.18. $Rexf_{avg}$ value for is equal to 13.20. For numerical simulation $Rexf_{avg}$ value is 13.01. The percentage differences between the two solution are acceptable, for Nusselt number and for friction factor too.

4. Thermo-physical properties of nanofluids

In this analysis both pure water and Al_2O_3/water based nanofluids with a particle diameter of 38 nm are considered as working fluid. The single-phase model approach is adopted in order to describe the nanofluid behavior because small temperature differences and small particle volume fractions are considered. In Table 2 the values of density, specific heat, dynamic viscosity and thermal conductivity, are reported for water and Al_2O_3 particles at the reference temperature of 293 K. In this paper different values of volume concentrations, equal to 0.1%, 0.5%, 1.0%, 2.0%, 4.0% and 4.0%, are investigated. Thermal properties are evaluated at a temperature equal to 293 K. Density was evaluated by using the classical formula valid for conventional solid-liquid mixtures while the specific heat and thermal expansion coefficient values are calculated by assuming the thermal equilibrium between nanoparticles and surrounding fluid. Thermal expansion coefficient values are evaluated by adopting the relation for different volume particle concentrations.

Density:

$$\rho_{nf} = (1-\varphi)\rho_{bf} + \varphi\rho_p \tag{11}$$

Specific heat:

$$\left(\rho c_p\right)_{nf} = (1-\varphi)\left(\rho c_p\right)_{bf} + \varphi\left(\rho c_p\right)_p \tag{12}$$

Thermal expansion coefficient:

$$\beta_{nf} / \beta_{bf} = \frac{1}{\left(\frac{1-\varphi}{\varphi}\frac{\rho_{bf}}{\rho_p}\right)}\frac{\beta_p}{\beta_{bf}} + \frac{1}{\left(\frac{\varphi}{1-\varphi}\frac{\rho_{bf}}{\rho_p}+1\right)} \tag{13}$$

Table 2. Material properties at the reference temperature of 293 K.

Material	ρ (kgm^{-3})	Cp (Jkg^{-1}K^{-1})	β (K^{-1})	μ (Pas)	λ (Wm^{-1}K^{-1})
Al_2O_3	3880	773	//	//	36
Water	998.2	4128	2.100x10^{-4}	993x10^{-4}	0.597

Viscosity and thermal conductivity are evaluated by means following equations, which are adopted because they are expressed as a function of particle volume concentration and diameter.

Dynamic viscosity:

$$\frac{\mu_{nf}}{\mu_{bf}} = \frac{1}{1-34.87\left(d_p / d_f\right)^{-0.3}\varphi^{1.03}} \tag{14}$$

with $d_f = 0.1\left(\frac{6M}{N\pi\rho_{f,0}}\right)$, in which M is the molecular weight of the base fluid, N is the Avogadro number and $\rho_{f,0}$ is the mass density of the base fluid calculated at T = 293 K.

Thermal conductivity:

$$\frac{\lambda_{nf}}{\lambda_{bf}} = 1 + 4.4\,\mathrm{Re}^{0.4}\,\mathrm{Pr}^{0.66}\left(\frac{T}{T_{fr}}\right)^{10}\left(\frac{\lambda_p}{\lambda_{bf}}\right)^{0.03}\varphi^{0.66} \tag{15}$$

with $\mathrm{Re} = \frac{2\rho_{bf}k_bT}{\pi\mu_{bf}{}^2 d_p}$, in which k_b is the Boltzmann constant, equal to 1.36x10^{-26}, and T_{fr} is equal to 273.15 K.

Validation has been accomplished by comparing the results at Re = 100 and Gr = 0 with literature, thermal boundary condition referring to constant axial wall heat flux with constant peripheral wall temperature [11]. In particular, the comparison in terms of local and average Nusselt number has been accomplished by considering data obtained by Wilbulswas [12] and also reported in [11]. Data are

presented as a function of the axial coordinate for the thermal entrance region, z^*, defined as $z^*=z/(dh$ Re). Furthermore, the validation in terms of friction factor has been performed by comparing data from Fleming and Sparrow [13], Miller and Han [14], and Aggarwala and Gangal [15], also reported in [11], with the obtained results for fully developed laminar flow in forced convection. Data reduction has been performed by considering the axial coordinate for the hydrodynamic entrance region, such as z^+ parameter, defined by $z^* = z/(dh\ Pe)$. Figure 2 shows these comparisons and it is clear that the present numerical results are in good agreement with the literature data. In particular, a maximum difference of 1.5% is observed for local and average Nusselt number at most, as shown in Figure 2a, while a maximum error of 2% is evaluated in terms of friction factor, as reported in Figure 2b. Thermal properties are evaluated at a temperature equal to 293 K and they are reported in Table 3

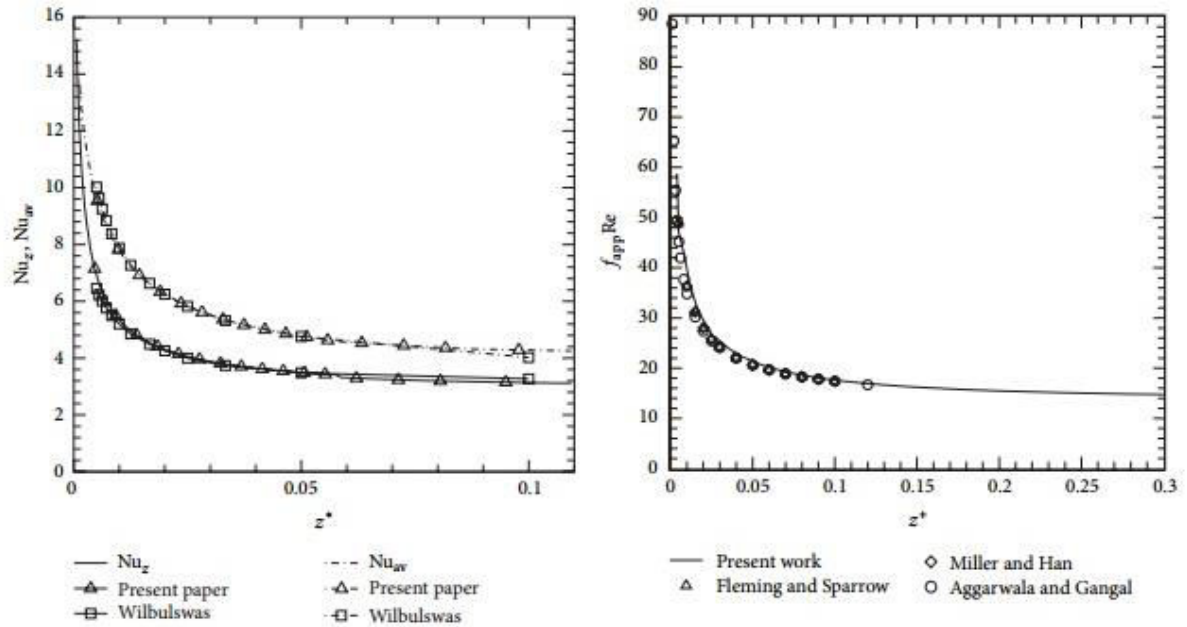

Figure 2. Validation pure water at *Re*=100 and *Gr*=0: a) average and local Nusselt number; b) f_{avg}xRe=f_{app}xRe

Table 3. Nanofluids properties at the reference temperature of 293 K.

Φ (%)	ρ (kgm^{-3})	Cp (Jkg^{-1}K^{-1})	λ (Wm^{-1} K^{-1})	μ (kgm^{-1} s^{-1})
0	998.2	4182	0.597	9.93x10^{-04}
0.1	1002	4179	0.599	1.00 x10^{-03}
0.5	1013	4117	0.611	1.03x10^{-03}
1.0	1027	4053	0.619	1.08x10^{-03}
2.0	1056	3931	0.632	1.18x10^{-03}
4.0	1113	3707	0.653	1.46x10^{-03}

5. Results

The results of the numerical simulations are carried out for q=7.56x10^{4}W/m^2, Reynolds number, *Re*, in the range 50-1000, Prandtl number in the range 6.96-8.29, and the nanoparticle volume fractions, ϕ, in the 0%-4.0% range. Different values of Grashof number, ranging from 0 to 5x10^6, were considered. Results are reported in terms of average convective heat transfer coefficient, average Nusselt number and required pumping power profiles.

In Fig. 3a average convective heat transfer coefficient profiles as a function of Reynolds number values for different nanoparticle volume fractions and thickness *S* are reported. For every Reynolds number nanofluids give an increment in the average convective coefficient respect to the one for the base fluid and this advantage is as greater as volume concentration of nanoparticle is. Besides, for each thickness *S* the convective coefficient increases approximately linearly as the Reynolds number increases. The effect of the value of the thickness *S* is very weak as expected because the microchannel wall is made of aluminum. Increment of average convective heat transfer coefficient due to the presence of nanoparticles is clear in Fig. 3b where the ratio between convective coefficients with and without nanoparticles inside the base fluid is reported as function of the Reynolds number. For each volume concentration the enhancement increases as the Reynolds number increases but this effect becomes weaker and weaker for high Reynolds numbers.

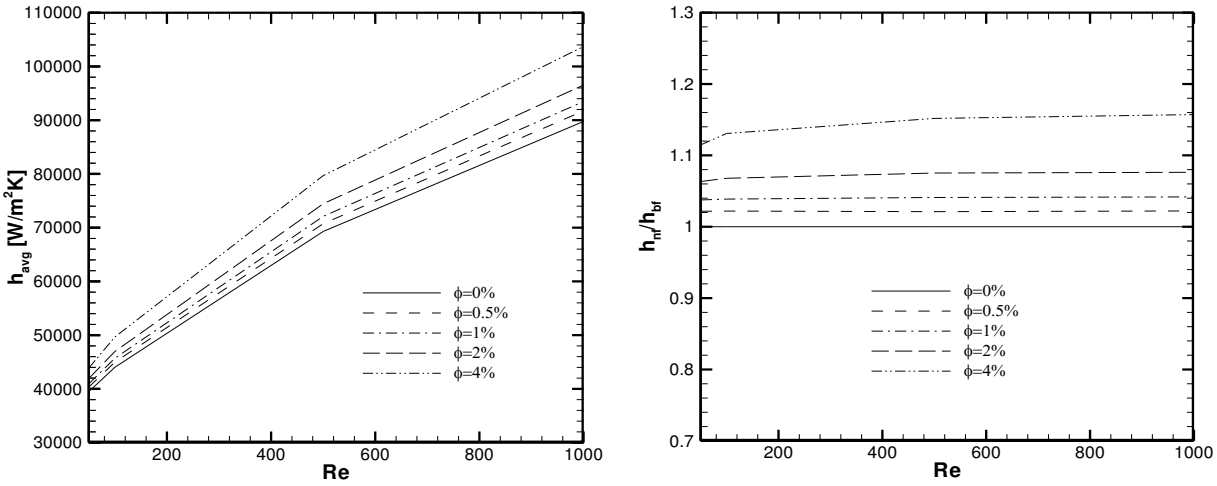

a) b)

Figure 3. Convective heat transfer coefficient for different volume fractions at varying of Reynolds number: a) absolute coefficient; b) relative coefficient

In Fig.4a average Nusselt number, which is defined in Eq.(8), as a function of the Reynolds number for *S*=6μm and different volume concentration is shown.

When the value of Reynolds number increases average Nusselt number increases too. For $\varphi \leq 0.5\%$

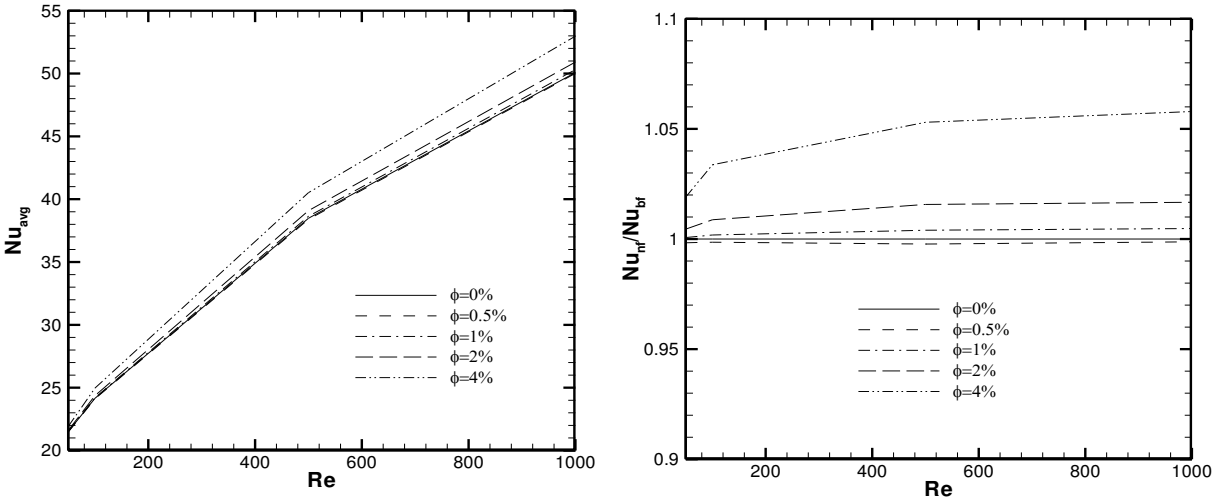

a) b)

Figure 4. Nusselt number for different volume fractions at varying of Reynolds number: a) absolute Nusselt number; b) relative Nusselt number.

Nusselt profiles are nearly overlapping. In addition, for $Re \leq 100$ average Nusselt numbers are very similar for all the investigated volume concentration values.

Indications of the effect of nanoparticles volume concentration on the augmentation of Nusselt number are given in Fig.4b. When volume concentration is lower 0.5%, average Nusselt number is nearly independent on the presence of nanoparticles and Reynolds number so it is very close to the value for pure water. For higher concentrations average Nusselt number increases as Reynolds number increases and this effect is stronger for $Re \leq 500$. Anyway the enhancement of the average Nusselt number is not marked. Maximum value of the Nu_{nf}/Nu_{bf} ratio is equal to 1.055 which is attained for φ=4.0% and Re=1000.

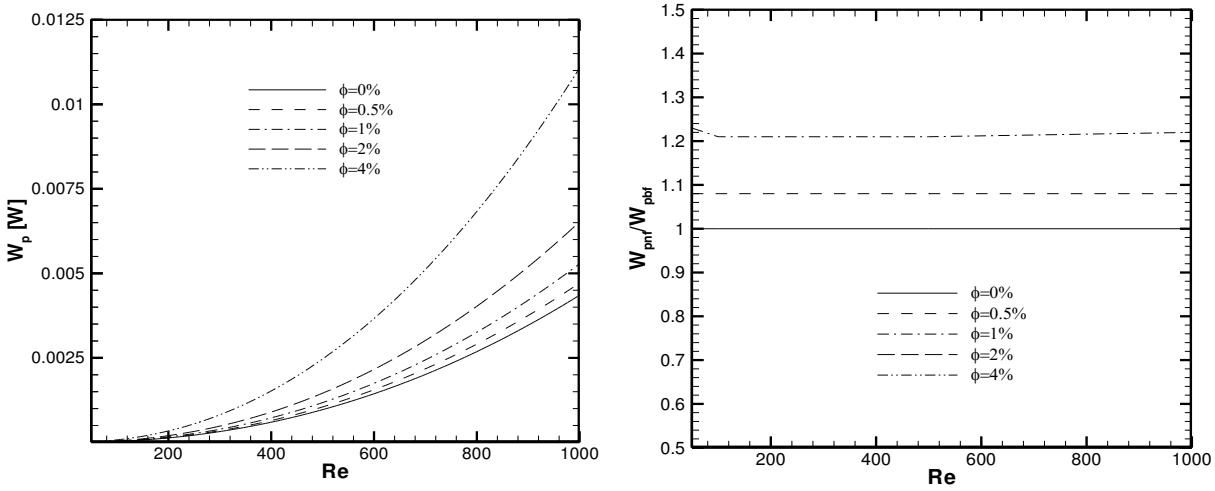

a) b)

Figure 5. a) Required pumping power as a function of Reynolds number; b) relative required pumping power as a function of Reynolds number

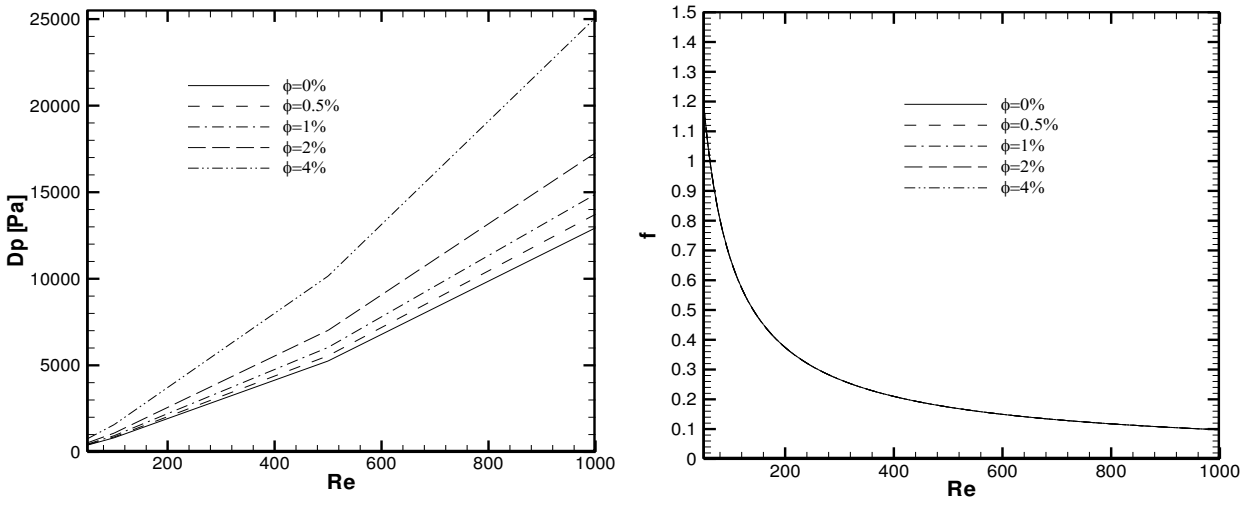

a) b)

Figure 6. a) Load losses as a function of the Reynolds number and for different volume concentrations of particles; b) friction factor as a function of Reynolds number

An interesting question is if the increase in the heat transfer performance due to the presence of nanoparticles does not require excessive pumping power. As an effect also pumping power strongly depends on particle volume concentration as shown in Fig.5a, particularly for $\varphi \leq 0.5\%$. Pumping

power enhancement as function of Reynolds number is shown in Fig.5b for several volume concentrations. This ratio for an assigned concentration is not dependent on Reynolds number. For φ=4.0% pumping power is 1.2 times the pumping power with pure water.

In Fig.6a pressure drop in the channel is reported as a function of Reynolds number for S=6μm and for different volume concentrations of nanoparticles. It is worth noticing that at an assigned Reynolds number pressure drop increases very quickly with particle volume concentration.

As far as the friction factor defined by Eq.(9), for a duct with rectangular cross section and for laminar flow and hydro-dynamically and thermally fully developed flow:

$$f=13.3/Re \tag{16}$$

In Fig.6b the friction factor as function of Reynolds number is reported for different volume concentrations. It is worth noticing that the friction factor is nearly independent on volume concentration. In conclusion the nanofluids have a higher capability to remove heat than pure fluid but this costs in terms of pumping power.

6. Conclusions

Results about the numerical analysis on laminar forced convection with nanofluids flowing in rectangular cross-sectioned ducts are presented in this paper. One of the walls is heated at uniform and constant heat flux. The investigation was carried out for $50 \leq Re \leq 1000$ and Al_2O_3/water based nanofluids at volume concentrations equal to 0%, 0.1%, 1%, 3% and 4%. The single-phase model was adopted in order to describe the behaviour of nanofluids as working fluids and thermo-physical properties were evaluated by means of equations, available in literature. The results showed the increase of the convective heat transfer coefficients, in particular, for high concentration of nanoparticles and for increasing values of Reynolds number.

The highest enhancement is evaluated for φ = 4% with the average convective heat transfer coefficient values equal to 1.14, 1.145, 1.147 times greater than the ones obtained for pure water, at Re =50, 500 and 1000, respectively. However, the disadvantages are represented by the growth of the wall shear stress and the required pumping power, observed in particular, at high particle concentrations.

Nomenclature

C_f	specific heat	Eq.(8)
d	Diameter	m
f	friction factor	Eq.(10)
H	duct height	m
l	duct edge length	m
L	total duct length	m
Nu	Nusselt number	Eq.(7)
P	pressure	Pa
Pr	Prandtl number	Eq.(11)
Re	Reynolds number	Eq.(6)
V	average velocity	m/s
$\dot{V}$	volume flow rate	m^3/s
W_p	pumping power	W
x, y, z	spatial coordinates	m
Greek symbols		
α	thermal diffusivity	m^2/s
β	volumetric expansion	1/K

	coefficient	
φ	nanoparticle volumetric concentration	
λ	thermal conductivity	W/m K
ν	kinematic viscosity	m^2/s
μ	dynamic viscosity	Pa s
ρ	density	kg/m^3
τ	wall shear stress	kg/m

Subscripts

avg	average
b_f	base fluid
f	fluid
h	hydraulic
I	inlet
m	mass
n_f	nanofluid
p	solid particle
w	wall

References

[1] Mohammed H A, Bhaskaran G, Shuaib N H, and Saidur R 2011 *Renew. Sust. Energy Rev.* **15** 1502.
[2] Lee S and Choi S U S, 1996 *ASME , Material Division (Publication) MD* **72** 227.
[3] Koo J, and Kleinstreuer C 2005 *Int. J. Heat Mass Transfer* **48** 2652.
[4] Chein R Y and Chuang J 2007 *Int. J. Therm. Science* **46** 57.
[5] Behzadmehr A, Saffar-Avval M and Galanis N 2007 *Int. J. Heat Fluid Flow* **28** 211.
[6] Jung J Y, Oh H S and Kwak H Y *2009 Int. J. Heat Mass Transfer* **52** 466.
[7] Bhattacharya P, Samanta A N and Chakraborty S 2009 *Heat Mass Transfer* **45** 1323.
[8] Chen C H and Ding C Y 2012 *Int. J. Therm. Science* **50** 378.
[9] Yang Y T, Tsai K T, Wang Y H and Lin S H 2014 *Int. Comm. Heat Mass Transfer* **57** 27.
[10] Fluent Inc. 2006 *FLUENT Computational Fluid Dynamic Code Version 6.3 User Guide*, www.fluent.com
[11] Shah R K and London A L 1978 Suppl. 1 *Advances in Heat Transfer*.
[12] Wilbulswas P 1966 Laminar-flow heat transfer in non-circular ducts [Ph.D. thesis], London University,
[13] Fleming D P and Sparrow E M 1969 *J. Heat Transfer* **91** 345.
[14] Miller R W and Han L S 1971 *J. Appl. Mech* **38** 1083.
[15] Aggarwala B D and Gangal M K 1975 *Trans. Can. Soc. Mech. Eng* **3** 231.